Collision effects in velocity-selective optical pumping of sodium

C. G. Aminoff, J. Javanainen, and M. Kaivola
Helsinki University of Technology, Department of Technical Physics, SF-02150 Espoo 15, Finland
(Received 17 June 1982)

We report on a quantitative experimental investigation of velocity-changing collisions by means of velocity-selective optical pumping (VSOP). We have calculated the VSOP line shape for an atom with hyperfine structure with the use of two phenomenological kernels for the collision effects: the Keilson-Storer kernel, and a two-term kernel consisting of a broad Keilson-Storer part and a narrower Gaussian component. Corrections were included to account for the finite absorption in the sample and the backward reflection of the pumping beam. The experiments were carried out in sodium vapor with neon as the perturber gas. The D_1 line of sodium was used for optical pumping, and the orientation of the ground state was detected. Free parameters of the theory were determined by fitting the predicted line shapes to experimental curves. The Keilson-Storer kernel proved unsatisfactory, but the two-term kernel reproduced well the observed line shapes over the entire collision profiles in the neon pressure range 0—57 mtorr. In an independent experiment using rapidly modulated VSOP we also measured directly the cross section of velocity-changing collisions: $\sigma=(1.13\pm0.10)\times10^{-14}$ cm^2. The large weight obtained for the narrow Gaussian from the fits, as well as the collision cross section which is three times as large as the cross section deduced from tabulated gas kinetic radii, may indicate the presence of collisions with relatively small velocity changes in addition to hard-sphere encounters.

I. INTRODUCTION

New and subtle techniques for the experimental investigation of atomic collision processes are provided by high-resolution laser spectroscopy. Any nonequilibrium distribution of atoms among the internal states and velocities in a gas will be affected by collisions. By the use of narrow-band lasers the effect of collisions on the atomic velocity distribution can be resolved inside a Doppler-broadened line. Information about the nature of the collision interaction itself can be derived from such observations.

In this work the method of velocity-selective optical pumping (VSOP) has been applied to investigate the velocity-changing effects of collisions between sodium atoms and neon perturbers. This technique utilizes the optical-pumping effect of a low-intensity light field on long-lived atomic states in combination with the high spectral resolution of a single-mode laser beam. Atomic observables (orientation, alignment, hyperfine population differences, etc.) can be created in the ground state or a metastable state in a narrow distribution of longitudinal velocities selected by the laser frequency. A counterpropagating detection beam interacting with the pumped atoms will consequently have its polarization or intensity modified. Doppler-free signals corresponding to the velocity distribution of anisotropy in the medium are then obtained by tuning the laser frequency. Collisions between atoms will produce a redistribution over velocities and possibly a depolarization of the atomic multipole components. The ensuing broad background in the spectrum reflects the characteristics of the collision interaction. The sensitivity of the VSOP signal to collision effects has already been qualitatively demonstrated in experiments on metastable states of neon.[1,2] The present paper reports on a systematic analysis of the velocity-changing effects of collisions appearing in the VSOP spectra of the D_1 line of sodium obtained with orientation.

A number of experimental results on velocity-changing collisions are already available in the literature (for reviews see Refs. 3 and 4). Various methods of saturation spectroscopy or two-photon spectroscopy have previously been applied, mostly including strong saturating laser fields. With the VSOP method applied in this work one avoids saturation of the optical transition and optical coherence effects. The evolution of the observables due to the interaction of the atoms with the light can be calculated exactly within the rate theory of optical pumping,[5] the essential new feature being the selec-

tion of a narrow group of velocities. In studying collisions within VSOP, only a single interatomic potential is involved and well-defined atomic observables are detected by applying modulation techniques. Thus, one avoids the mixing of contributions from different electronic levels and from various atomic multipole components having different collisional relaxation characteristics. Such features, often inherent in saturation spectroscopy, complicate an accurate interpretation of the line shapes.

At present a practical approach to the theoretical analysis of velocity-changing collisions seems to be restricted to phenomenological collision models used with kinetic equations of the Boltzmann type. In several detailed studies a hard-sphere collision model has been applied for comparison with experimental line shapes.[6–9] The hard-sphere approach appears to be satisfactory for collisions with very light perturber atoms that are able to produce only small velocity changes in a single collision.[9] In such experiments the detailed features of the collision kernel are not easily resolved. On the other hand, collisions with heavy perturbers have been described as predominantly "strong" and rapidly thermalizing.[6,8,9]

Sodium atoms colliding with neon perturbers of nearly equal mass represent an interesting intermediate case characterized by progressive thermalization but still having a clearly resolved average velocity change per collision. Effects of rare-gas collisions on the excited $3P_{1/2}$ state of sodium have previously been studied in a two-photon experiment[9] where hard-sphere models were applied. We have analyzed our VSOP spectra of sodium using collision models with varying parameters to allow for deviations from the hard-sphere character. In this paper a two-term collision kernel is discussed that includes large-angle scattering as well as smaller velocity changes with enhanced persistence of velocity. Corrections to the line profiles accounting for the absorption of the light beams and the retroreflection of the pumping beam have been included in the analysis. A detailed comparison of the new model kernel with experimental results has been performed and values for characteristic parameters have been determined.

We have also measured the cross section for velocity changes of sodium colliding with neon atoms in an independent experiment applying rapidly modulated VSOP and a phase-shift method.[2]

Section II contains an outline of the VSOP theory applied to an atom with hyperfine structure. Collision effects are included and line shapes are given. Model kernels for velocity-changing collisions are considered in Sec. III. Details of the experiments and results are reported in Sec. IV. Experimental line shapes are compared with theory in Sec. V, followed by a concluding discussion in Sec. VI.

II. VSOP IN ATOMS WITH HYPERFINE STRUCTURE

A. The rate equation

Optical pumping produced by a low-intensity light wave may cause significant modifications of Zeeman sublevel populations in a long-lived atomic state without noticeable changes in the populations of the electronic levels of the atom. The rate theory of optical pumping with discharge light sources is well established.[5,10] When the linewidth of the light is much smaller than the Doppler broadening in a gas, the pumping acts selectively on a single velocity group of atoms, introducing a correlation between internal variables and atomic velocities. We consider a monochromatic light field

$$\vec{\mathscr{E}}(\vec{r},t)=\vec{e}_\lambda \mathscr{E}\exp[i(\vec{k}\cdot\vec{r}-\Omega t)]+\text{c.c.} \tag{1}$$

with polarization $\vec{e}_\lambda$, angular frequency Ω, and wave vector $\vec{k}$. The field interacting with an atom is assumed to be weak enough to satisfy the condition

$$|\vec{\mathscr{D}}\cdot\vec{\mathscr{E}}| \ll \hbar\Gamma_{eg}\ , \tag{2}$$

where $\vec{\mathscr{D}}$ is the atomic dipole moment and Γ_{eg} is the homogeneous linewidth of the atomic transition. In this limit we may neglect coherence effects in the evolution of the atomic density matrix, and the rate equations for optical pumping are still valid.

The hyperfine structure exhibited, for instance, by alkali-metal atoms introduces some additional complexity into the high-resolution spectrum. Within VSOP, however, it is straightforward to calculate exactly the various contributions to the signal from the spectral components. When the hyperfine splitting is of the order of the Doppler width, the structure of the atomic levels will not only lead to a splitting of the line, but also introduce additional crossover resonances due to the experimental geometry.

Consider an atomic system consisting of two electronic energy levels with angular momenta J_g and J_e in the ground and excited states, respectively. The nuclear spin I leads to hyperfine splitting into sublevels characterized by total angular momenta F_μ in the excited state and F_ν in the ground state, see Fig. 1(a). The energy difference between the levels F_μ and F_ν is denoted by $\hbar\Omega_{\mu\nu}$. Monochromatic pumping and detection beams are propagating in op-

posite directions through a cell containing the gas [see Fig. 1(b)].

We will explicitly consider only the axial velocity component v of the atom. Associating velocity-dependent density matrices $\rho_\mu(v)$ and $\rho_\nu(v)$ with the atoms on the levels F_μ and F_ν, respectively, we generalize the VSOP equations of Ref. 2 to include the hyperfine structure. In the absence of collisions in the gas and without magnetic fields we obtain

$$\frac{d}{dt}\rho_\nu(v,t) = -\sum_\mu \left(\tfrac{1}{2}\gamma_p^{\mu\nu}(v)\{B_{\mu\nu},\rho_\nu(v,t)\}_+ + i\Delta E^{\mu\nu}(v)[B_{\mu\nu},\rho_\nu(v,t)]\right) + \sum_\mu \Gamma_{\mu\nu} \sum_{i=xyz} D_i\rho_\mu(v,t)D_i - \gamma_0[\rho_\nu(v,t)-\rho_\nu^0(v)] , \tag{3a}$$

$$\frac{d}{dt}\rho_\mu(v,t) = \sum_\nu \gamma_p^{\mu\nu}(v)(\vec{e}_\lambda\cdot\vec{D})\rho_\nu(v,t)(\vec{e}^{\,*}_\lambda\cdot\vec{D}) - \Gamma_\mu\rho_\mu(v,t) , \tag{3b}$$

where the sum over μ (ν) is taken over the hyperfine levels F_μ (F_ν) of the excited (ground) state. The absorption rate $\gamma_p^{\mu\nu}(v)$ and the light shift $\Delta E^{\mu\nu}(v)$ for the transition $F_\nu \rightarrow F_\mu$ are determined by the real and imaginary parts, respectively, of the expression

$$\tfrac{1}{2}\gamma_p^{\mu\nu}(v) + i\Delta E^{\mu\nu}(v) = i\frac{|\mathscr{E}|^2|\mathscr{D}_{eg}|^2}{\hbar^2(2J_e+1)}(\Omega-\Omega_{\mu\nu}-kv+i\Gamma_{eg})^{-1} , \tag{4}$$

where $\mathscr{D}_{eg}$ is the reduced matrix element of the dipole moment

$$\mathscr{D}_{eg} = \langle J_e||\vec{\mathscr{D}}||J_g\rangle . \tag{5}$$

The rate of decay from the level F_μ to F_ν through spontaneous emission is $\Gamma_{\mu\nu}$ and the total spontaneous decay rate of the level F_μ is $\Gamma_\mu = \sum_\nu \Gamma_{\mu\nu}$. The absorption operator $B_{\mu\nu}$ is defined by

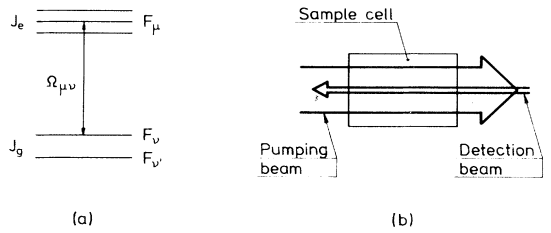

FIG. 1. (a) Atomic system with hyperfine structure. J_e and J_g are the electronic angular momenta of the ground state and excited state, respectively. Total angular momenta of the hyperfine levels are denoted by F_μ for the excited state and F_ν for the ground state. Resonance angular frequency for the transition between F_ν and F_μ is $\Omega_{\mu\nu}$. (b) Scheme for velocity-selective optical pumping. Pumping beam is expanded to provide homogeneous optical-pumping conditions. Sample is probed by a counterpropagating detection beam.

$$B_{\mu\nu} = P_\nu(\vec{e}^{\,*}_\lambda\cdot\vec{D})P_\mu(\vec{e}_\lambda\cdot\vec{D})P_\nu , \tag{6}$$

where $P_{\mu,\nu}$ are projection operators onto the states $F_{\mu,\nu}$ and $\vec{D}$ is a vector operator containing only the angular part of $\vec{\mathscr{D}}$. In defining (4) we have used the fact that the dipole operator $\vec{\mathscr{D}}$ acts only on the variables of the electrons and not on those of the nucleus (cf. Appendix A).

The anticommutator and the commutator in (3a) describe the effects of absorption and light shifts, respectively, on the hyperfine levels of the ground state. The term in (3a) containing $\Gamma_{\mu\nu}$ and that in (3b) proportional to Γ_μ give the effect of spontaneous emission. The last term on the right-hand side (rhs) of (3a) describes the relaxation of the ground-state density matrix towards thermal equilibrium due to the fact that the atoms enter and leave the beam, which takes place at a rate $\gamma_0 \ll \Gamma_\mu$. Finally, the first term on the rhs of (3b) contains the transfer of atoms from the ground state to the excited state by absorption. The thermal equilibrium density matrix is written

$$\rho_\nu^0(v) = [(2I+1)(2J_g+1)]^{-1}N(v)\mathbb{1} \tag{7a}$$

with $N(v)$ given by the Maxwellian distribution

$$N(v) = \frac{N_0}{\sqrt{\pi}\,u}\exp\left[-\left[\frac{v}{u}\right]^2\right] , \tag{7b}$$

where N_0 is the atomic number density and u is the most probable speed.

For a low intensity of the pumping light, such that $\gamma_p^{\mu\nu} \ll \gamma_0$, Eqs. (3) can be written to first order in the pumping rate for a description of the effect of optical pumping on the ground levels (see Appendix A). To the lowest order the light-shift term vanishes. The resulting linearized equations of motion for the density matrix allow us to calculate the evolution of the atomic observables of the hyperfine levels (orientation, alignment, and hyperfine popula-

tion differences) under the influence of velocity-selective optical pumping. In order to study the orientation F_z of the hyperfine level F_ν of the ground state we calculate the velocity-dependent expectation value

$$\langle F_z\rangle_\nu(v)=\mathrm{Tr}_\nu\{F_z\rho_\nu(v)\}\ , \tag{8}$$

where the trace runs over the Zeeman sublevels of the hyperfine state F_ν. For the equation of motion we obtain (see Appendix A)

$$\frac{d}{dt}\langle F_z\rangle_\nu(v,t)=\bar{\gamma}_p\langle F_z\rangle_{p\nu}(v)-\gamma_0\langle F_z\rangle_\nu(v,t)\ . \tag{9}$$

The total orientation distribution of the atom is given by

$$\langle F_z\rangle(v,t)=\sum_\nu\langle F_z\rangle_\nu(v,t)\ , \tag{10}$$

where the sum is taken over the ground-state hyperfine levels F_ν. The constant pumping rate $\bar{\gamma}_p$ is defined by

$$\bar{\gamma}_p=2\,|\,\mathscr{E}\,|^2\,|\,\mathscr{D}_{eg}\,|^2/(2J_e+1)\hbar^2\Gamma_{eg}\ . \tag{11}$$

The distribution of $\langle F_z\rangle_\nu(v)$ is essentially determined by the source term

$$\langle F_z\rangle_{p\nu}(v)=N(v)\sum_{\mu\nu'}\langle F_z\rangle_{p\nu}^{\mu\nu'}L(\Omega-\Omega_{\mu\nu'}-kv)\ , \tag{12}$$

where $L(x)$ is the Lorentzian function

$$L(x)=\Gamma_{eg}^2/(x^2+\Gamma_{eg}^2)\ . \tag{13}$$

The pumping coefficients $\langle F_z\rangle_{p\nu}^{\mu\nu'}$ in (12) are given in Appendix A. The indices μ,ν,ν' label the hyperfine levels involved: The orientation of the level F_ν is achieved by excitation from $F_{\nu'}$ to F_μ, followed by transfer through spontaneous emission to the level F_ν in the velocity group determined by $v=(\Omega-\Omega_{\mu\nu'})/k$. The branching of the spontaneous decay towards different hyperfine levels leads to repopulation pumping effects when $\nu\neq\nu'$.

The stationary solution of (9) gives the velocity distribution of $\langle F_z\rangle$ on the ground levels. This is formed by narrow Lorentzians of width $2\Gamma_{eg}/k$, as is seen from (12). Equation (9) allows us to exactly calculate the relative strengths of all the hyperfine components in the orientation spectrum. The observables of the excited state will give relative contributions, proportional to γ_0/Γ_μ, to the VSOP signal and can be neglected when $\gamma_0\ll\Gamma_\mu$.

B. The signal

The VSOP signal is obtained by detecting the modification of the transmitted counterpropagating probe beam [see Fig. 1(b)]. In the present experiment the polarization of the pumping beam is modulated between the right- and left-circular states $\sigma_\pm$. This gives rise to a time-varying circular dichroism which appears as a modulation in the absorption of the circularly polarized detection beam.

To calculate the ac signal we apply the formalism of Ref. 2 to an atom with hyperfine structure (see Appendix B). The signal proportional to the orientation of the ground level is given by

$$S(\Omega)\propto|\,\mathscr{E}_d\,|^2\,|\,\mathscr{D}_{eg}\,|^2\sum_{\mu\nu}R_{\mu\nu}^{(1)}\int_{-\infty}^{\infty}dv\langle F_z\rangle_\nu(v)L(\Omega-\Omega_{\mu\nu}+kv)\ , \tag{14}$$

where the sum is taken over hyperfine levels μ,ν. The detection beam has the field strength $\mathscr{E}_d$ and the same angular frequency Ω as the pumping beam. The factor $R_{\mu\nu}^{(1)}$, defined in Appendix B, determines the relative contribution to the orientation signal from the probe beam absorption for each transition $F_\nu\rightarrow F_\mu$. This factor is obtained by decomposing the F states, as the dipole operator acts only on electronic variables. The orientation is probed in narrow Doppler-shifted velocity groups determined by the Lorentzians in (14).

An explicit expression is obtained by inserting into (14) the orientation distribution $\langle F_z\rangle_\nu(v)$ from the stationary solution of (9). Assuming $\Gamma_{eg}\ll ku$ (Doppler limit) we have, after integration,

$$S(\Omega)\propto|\,\mathscr{E}_d\,|^2\,|\,\mathscr{D}_{eg}\,|^2\frac{\bar{\gamma}_p}{\gamma_0}\sum_{\mu\nu}\sum_{\mu'\nu'}Q_{\mu\nu}^{\mu'\nu'}L(\Omega-\tfrac{1}{2}(\Omega_{\mu\nu}+\Omega_{\mu'\nu'}))\exp\left[-\left[\frac{\Omega_{\mu\nu}-\Omega_{\mu'\nu'}}{2ku}\right]^2\right] \tag{15}$$

with

$$Q_{\mu\nu}^{\mu'\nu'}=R_{\mu\nu}^{(1)}\langle F_z\rangle_{p\nu}^{\mu'\nu'}\ . \tag{16}$$

The factors (16) give the relative strengths of the Doppler-free hyperfine structure resonances in the VSOP signal described by (15). The "direct" hyperfine resonances involve two-level transitions with $\mu=\mu'$ and $\nu=\nu'$. The resonances with $\mu\neq\mu'$ and/or $\nu\neq\nu'$ are crossover processes that involve three or four levels and appear at half the sum frequency of any pair of transitions. Analogous crossover signals are familiar in saturated absorption

spectroscopy. In VSOP the crossover signals are particularly simple to interpret quantitatively. For a resonance with $\nu \neq \nu'$ (different lower levels) the detection beam probes only the effect of repopulation pumping produced in the branching of spontaneous decay. Owing to the symmetric dependence of (15) on $\Omega_{\mu\nu}$ and $\Omega_{\mu'\nu'}$ some of the resonances coincide.

C. Collisions and line shapes

Although the vapor pressure of the active atoms is low enough to allow a mean free path much longer than the cell, the presence of a buffer gas will give rise to collisions between active atoms and perturbers that change the atomic velocities. A pumped atom in the ground state has a long effective lifetime in the beam and is apt to undergo several collisions even in low perturber gas pressures. This leads to a spreading of pumped atoms over velocities. In fact, strong collisions may result in optical pumping of the entire Doppler profile.[11,12] The VSOP line shapes contain information about the relaxation characteristics of the multipole components of the atomic density matrix as well as velocity-changing effects.

We assume the collisional relaxation to be isotropic and neglect any collisional coupling between observables of different multipolarity. The perturber pressure is assumed low enough to allow us to neglect collisions during the lifetime of the excited state, i.e., $\gamma_c \ll \Gamma_\mu$, where γ_c is the collision rate.[13] The orientation $\langle F_z \rangle_\nu(v')$ of the atoms with axial velocity v' on each hyperfine level F_ν of the ground state is transferred by a collision to the velocity v at a rate given by the collision kernel $K(v',v)$. A one-dimensional description of the kernel will be used, and $K(v',v)$ is taken to be identical for all hyperfine levels F_ν. The equation of motion for the ground-state orientation $\langle F_z \rangle_\nu(v)$ including collision effects is obtained from (9) by adding collision rate terms. We find the transport equation

$$\frac{d}{dt}\langle F_z \rangle_\nu(v) = \bar{\gamma}_p \langle F_z \rangle_{p\nu}(v) - \gamma \langle F_z \rangle_\nu(v) + \int_{-\infty}^{\infty} dv' \langle F_z \rangle_\nu(v') K(v',v) \ . \quad (17)$$

The rate of relaxation for each velocity group is

$$\gamma = \gamma_0 + \gamma_c \ , \quad (18)$$

where the collision rate γ_c is taken to be independent of velocity.[14] The kernel $K(v',v)$ describes the disorienting effect as well as the velocity change. We define

$$\int_{-\infty}^{\infty} K(v',v)dv = \xi \gamma_c \ , \quad (19)$$

where ξ is a parameter giving the fraction of orientation conserved in a collision ($0 \leq \xi \leq 1$).

The formal steady-state solution of (17) is obtained by iteration (see, e.g., Ref. 3). We write the solution for the orientation distribution in the form

$$\langle F_z \rangle_\nu(v) = \frac{\bar{\gamma}_p}{\gamma} \sum_{\mu\nu'} \langle F_z \rangle_{p\nu}^{\mu\nu'} [N(v) L(\Omega - \Omega_{\mu\nu'} - kv) + \sum_{n=1}^{\infty} \Phi_{\mu\nu'}^{(n)}(v)] \ , \quad (20)$$

where

$$\Phi_{\mu\nu'}^{(n)}(v) = \gamma^{-1} \int_{-\infty}^{\infty} dv' N(v') L(\Omega - \Omega_{\mu\nu'} - kv') \times K^{(n)}(v',v) \ . \quad (21)$$

We have defined the convolutions

$$K^{(n)}(v',v) = \gamma^{-1} \int_{-\infty}^{\infty} dv_1 K^{(n-1)}(v',v_1) K(v_1,v) \ , \quad (22a)$$

$$K^{(1)}(v',v) = K(v',v) \ . \quad (22b)$$

The first term on the rhs of (20) gives the orientation of atoms that have not collided, and the sum term describes the collisional redistribution over velocities. The function $\Phi_{\mu\nu'}^{(n)}(v)$ gives the probability distribution for the orientation of an atom after n successive collisions.

We will not consider very weak collisions, i.e., we assume that the width of the kernel is clearly larger than the homogeneous linewidth $2\Gamma_{eg}/k$. The detected orientation signal is then found from (14) and (20) after integration:

$$S(\Omega) \propto \frac{\bar{\gamma}_p}{\gamma} \sum_{\mu\nu} \sum_{\mu'\nu'} Q_{\mu\nu}^{\mu'\nu'} \exp\left[-\left[\frac{\Omega - \Omega_{\mu'\nu'}}{ku} \right]^2 \right] \left[L(\Omega - \tfrac{1}{2}[\Omega_{\mu\nu} + \Omega_{\mu'\nu'}]) + 2\pi \frac{\Gamma_{eg}}{k\gamma} \sum_{n=1}^{\infty} K^{(n)}(v_{\mu'\nu'}, -v_{\mu\nu}) \right] \quad (23)$$

with the definition

$$v_{\mu\nu} = (\Omega - \Omega_{\mu\nu})/k \ . \quad (24)$$

The signal (23) is seen to contain a spectrum of narrow resonances superposed on broader background distributions produced by collisions and described by

the sum over n. Once the kernel $K(v',v)$ is known, the complete VSOP line shape is given by (23).

D. Modulated VSOP and the collision rate

Fast modulation of the optical pumping, a variant of the VSOP method,[2,15] permits a direct measurement of the collision rate γ_c. When the modulation frequency becomes comparable to the characteristic relaxation rate of the observable, a modification of the signal takes place. This phenomenon gives access to γ_c.

Modulating the pumping polarization at the angular frequency ω introduces a complex relaxation rate $\gamma+i\omega$ into (17) and leads to a dephasing of the signal. The complex solution of (17) acquires the form

$$\langle F_z\rangle_v(v,t)=\frac{\bar{\gamma}_p}{\gamma+i\omega}e^{i\omega t}\sum_{\mu\nu'}\langle F_z\rangle_{pv}^{\mu\nu'}[N(v)L(\Omega-\Omega_{\mu\nu'}-kv)+\mathcal{F}(\omega,v)]\ , \tag{25}$$

where $\mathcal{F}(\omega,v)$ accounts for the modified collision background (for details see Ref. 2). Thus a phase shift is introduced in $\langle F_z\rangle_v$. By extracting a single Lorentzian resonance from the background we find, for the signal determined by the real part of (25),

$$S^R_{\mu\nu}(\Omega,t)\propto\frac{\bar{\gamma}_p}{\gamma^2+\omega^2}(\gamma\cos\omega t+\omega\sin\omega t)\times Q^{\mu\nu}_{\mu\nu}L(\Omega-\Omega_{\mu\nu})\ . \tag{26}$$

A measurement of the amplitudes of the in-phase and in-quadrature components of the phase-shifted peak (26) yields the ratio

$$(S^R_{\pi/2}/S^R_0)_{\mu\nu}=\frac{\omega}{\gamma}\ . \tag{27}$$

This provides the value of γ, and γ_c is subsequently obtained from the linear variation of γ as a function of pressure. This method is sensitive to collisions producing a resolved average velocity change $\Delta v>2\Gamma_{eg}/k$.

III. THE COLLISION KERNEL

Complete knowledge of the collision kernel would imply a mastery of the collision process. However, purely theoretical kernels are at present restricted to simple models like hard-sphere collisions, and experimental maps of kernels are not directly available. Our approach is to choose suitable functional forms for the kernel shape and compare the ensuing theoretical line shapes with experiments. This procedure allows us to elucidate some characteristics of the collisions.

The choice of model kernels is restricted because it is difficult to extract numerical results from the iterative solution (20), unless the integral in (22a) can be evaluated analytically. A common phenomenological ansatz is the Keilson-Storer kernel[16] which we write

$$K_s(v',v)=\frac{\xi\gamma_c}{\sqrt{\pi}\beta}\exp\left[-\left[\frac{v-\alpha v'}{\beta}\right]^2\right] \tag{28}$$

with $\beta=(1-\alpha^2)^{1/2}u$. This kernel has the form of a displaced Gaussian distribution with a velocity shift determined by α. The Keilson-Storer kernel yields analytically tractable solutions for the line shape and gives a thermal distribution of atomic velocities in the limit when a large number of collisions take place.

The width parameter α depends on the active atom-perturber mass ratio and gives a measure of the strength of the collision or the amount of "velocity memory" retained in a collision. For $\alpha=0$ the collision is thermalizing.

The Keilson-Storer model (28) leads to VSOP line shapes obtained from (23), where the collision background is given by the sum of the terms

$$2\pi\frac{\Gamma_{eg}}{k\gamma}\exp\left[-\left[\frac{\Omega-\Omega_{\mu'\nu'}}{ku}\right]^2\right]K_s^{(n)}(v_{\mu'\nu'},-v_{\mu\nu})$$
$$=2\sqrt{\pi}\frac{\Gamma_{eg}}{ku}\left[\frac{\xi\gamma_c}{\gamma}\right]^n(1-\alpha^{2n})^{-1/2}\times\exp[-f^{(n)}(v_{\mu'\nu'},v_{\mu\nu})] \tag{29}$$

with

$$f^{(n)}(v_{\mu'\nu'},v_{\mu\nu})=\frac{v^2_{\mu\nu}+2\alpha^n v_{\mu\nu}v_{\mu'\nu'}+v^2_{\mu'\nu'}}{(1-\alpha^{2n})u^2}\ . \tag{30}$$

The profile described by (29) and (30) also includes the contributions from crossover processes.

In a few previous studies of velocity-changing collisions the Keilson-Storer kernel has been used with a fixed value of α to approximate the effects of a hard-sphere potential.[7–9,17] In experiments on excited sodium atoms with rare-gas perturbers,[9] the hard-sphere approximation described large-angle

scattering adequately, but for heavy perturbers it failed to reproduce the relatively small velocity changes contributing in the vicinity of the resonance. An additional narrow part in the kernel corresponding to collisions occurring with large impact parameters has also been found in saturated absorption experiments.[18,19] In effect, a narrow kernel depending only on the difference $|v-v'|$ has been proposed to describe weak collisions in low pressures.[19,20]

In order to describe the manifestations of collisions in VSOP spectra of sodium we will adopt two alternative approaches. First, we compare the experimental results with the Keilson-Storer model using a freely adjustable value of α. Second, we will use a more complex model kernel which explicitly accounts for additional scattering effects near the resonance velocity. We consider a two-term collision kernel of the form

$$K_c(v',v)=\epsilon G(v',v)+(1-\epsilon)K_s(v',v) , \tag{31}$$

where $G(v',v)$ is chosen as

$$G(v',v)=\frac{\xi\gamma_c}{\sqrt{\pi}\,\delta}\exp\left[-\left[\frac{v-v'}{\delta}\right]^2\right] \tag{32}$$

and $K_s(v',v)$ is given by (28). This model introduces two additional parameters into the problem: ϵ determines the relative weights of the two terms, and δ gives the width of $G(v',v)$. The first term in (31), a Gaussian symmetric in v and v', is taken to be narrow with respect to the Keilson-Storer part[21]:

$$\delta \ll \beta . \tag{33}$$

In general, a two-term kernel of the form (31) leads to cumbersome double sums in the iterative solution of (17). However, under the condition (33) a useful approximation can be developed. Loosely speaking, we may then state that the effect of any number of collisions associated with the narrow Gaussian kernel is masked by even a single collision taking place according to the broad Keilson-Storer kernel. Quantitatively, we assume that we have iterated K_c n times and decomposed the result into two parts

$$K_c^{(n)}(v',v)\simeq g^{(n)}(v',v)+k_s^{(n)}(v',v) , \tag{34}$$

where $k_s^{(n)}$ ($g^{(n)}$) only contains iterated Keilson-Storer (Gaussian) kernels. The next approximation is determined as follows. We write

$$\begin{aligned}K_c^{(n+1)}(v',v)&\simeq\gamma^{-1}\int dv_1[g^{(n)}(v',v_1)+k_s^{(n)}(v',v_1)][\epsilon G(v_1,v)+(1-\epsilon)K_s(v_1,v)]\\&\simeq\frac{\epsilon}{\gamma}\int dv_1 g^{(n)}(v',v_1)G(v_1,v)+\epsilon\frac{\xi\gamma_c}{\gamma}k_s^{(n)}(v',v)+(1-\epsilon)K_s(v',v)\int dv_1 g^{(n)}(v',v_1)\\&\quad+(1-\epsilon)\frac{1}{\gamma}\int dv_1 k_s^{(n)}(v',v_1)K_s(v_1,v) .\end{aligned} \tag{35}$$

The first term is $g^{(n+1)}$, and the sum of the last three terms defines $k_s^{(n+1)}$. By induction we obtain

$$\begin{aligned}&K_c^{(n)}(v',v)\\&\quad=\epsilon^n G^{(n)}(v',v)\\&\qquad+\sum_{m=1}^{n}\begin{bmatrix}n\\m\end{bmatrix}(\epsilon\eta)^{n-m}(1-\epsilon)^m K_s^{(m)}(v',v) ,\end{aligned} \tag{36}$$

where we have defined $\eta=\xi\gamma_c/\gamma$, and

$$G^{(n)}(v',v)=\frac{\gamma}{\sqrt{\pi n}\,\delta}\eta^n\exp\left[-\frac{(v-v')^2}{n\delta^2}\right] , \tag{37}$$

$$\begin{aligned}&K_s^{(m)}(v',v)\\&\quad=\frac{\gamma}{\sqrt{\pi}\,u}\eta^m(1-\alpha^{2m})^{1/2}\exp\left[-\frac{(v-\alpha^m v')^2}{(1-\alpha^{2m})u^2}\right] .\end{aligned} \tag{38}$$

The steady-state velocity distribution is the sum of (36) over $n=1,2,\ldots$. This can be cast into a simple form by changing the order of summation in the second term:

$$\begin{aligned}&\sum_{n=1}^{\infty}K_c^{(n)}(v',v)\\&\quad=\sum_{m=1}^{\infty}\left[\epsilon^m G^{(m)}(v',v)\right.\\&\qquad\left.+\frac{1}{1-\epsilon\eta}\left[\frac{1-\epsilon}{1-\epsilon\eta}\right]^m K_s^{(m)}(v',v)\right] .\end{aligned} \tag{39}$$

We have used the running integer m on the rhs of (39) to emphasize that there is no longer a unique correspondence between the summing index and the number of collisions n.

Although the kernel (31) does not give the thermal distribution of velocities in the limit of a large number of collisions, the approximate sum (39)

does. In fact, for increasing pressure we have $\eta \to 1$, and for any ϵ such that $0 \leq \epsilon < 1$ the Keilson-Storer part finally dominates. On the other hand, letting $\gamma_c \to 0$ the rhs of (39) reproduces the initial kernel (31).

The form (39) permits a numerical evaluation of the collision line shape without an excessive use of computer time. Our approximation scheme can generally be applied to any functional form of the two-term kernel. When the broad term asymptotically gives a thermal distribution at high pressures, so does the approximate expression corresponding to (39), and in the limit of low pressures it gives back the assumed two-term kernel. The buildup of a narrow part in the velocity distribution may even be described with a model that would not give the thermal limit, since this shortcoming is removed in the expression (39) giving the total steady-state distribution produced by collisions. In particular, when the calculation leading to (39) is repeated with an immediately thermalizing kernel as the broad part, and a Keilson-Storer form of arbitrary width as the "narrow" part, it gives the exact result.[18]

We have chosen the Keilson-Storer form for the broad part of the kernel because it is the only nontrivial kernel shape known that gives both analytically tractable results and the correct thermal limit. Its relation to hard-sphere models has also been studied in some detail.[8,9,17] For the narrow part we have wanted to choose a smooth kernel that shows an enhanced persistence of velocity and is also easy to handle numerically. These arguments suggest a kernel of the form $f(|v-v'|)$, and we have rather arbitrarily chosen the Gaussian (32) to describe our experimental data.

IV. EXPERIMENTS

A. The VSOP spectrum of sodium

The VSOP experiment was performed with orientation in the sodium ground state by using the D_1 line (589.6 nm). The collision studies were carried out with neon as the perturber gas. The density of sodium was kept low enough for collisions between sodium atoms to be negligible.

Details of the experimental scheme are shown in Fig. 2. The cylindrical Pyrex cell, 30 mm long and 20 mm in diameter, was connected to a vacuum line for evacuation and filling with neon. The cell was placed in an oven heated with a coaxial heating wire (Thermocoax) to minimize stray magnetic fields. The temperature was kept at about 150 °C and was stabilized to within 1 °C. A drop of sodium metal was contained in a "coldfinger" surrounded by a smaller oven compartment with an independent heating system. This allowed the temperature in the finger to be kept somewhat lower than in the cell in order to avoid sodium deposit on the windows and to limit the absorption to not more than 25% at line maximum. This corresponds to a density of sodium of approximately 2×10^{10} cm^{-3} or a pressure of 10^{-6} torr.

The light source was a cw dye laser (Spectra Physics 375). Tunable single-mode operation was accomplished by using a double Michelson mode selector.[22] The effective linewidth of the free running laser was about 10 MHz. The dye-laser intensity was stabilized against slow drift by a servo control of the Ar^+ pump laser power. The pumping beam was expanded to a diameter of 7 mm, and its polarization was modulated between right- and left-handed circular states at a frequency of about 130 Hz by an electro-optic crystal. The detection beam originating from the same laser was about 2 mm in diameter and was circularly polarized by a $\lambda/4$ retarder. The beam was split into two beams of equal intensity before the cell to enable differential detection. The pumped dichroism in the vapor produced a signal in the transmitted probe beam intensity, which was demodulated by a lock-in amplifier. The resulting signal was recorded as a function of laser frequency.

The intensity of the pumping beam was attenuated to 0.6 μW/mm^2 and that of the detection beam to 0.3 μW/mm^2 in order to avoid any saturation of the signal and to assure operation in the optical-pumping regime.[23] The pumping intensity corresponds to $\bar{\gamma}_p \sim 10^5$ s^{-1} which yields $\bar{\gamma}_p/\gamma_0 < 1$, and by evaluating $\langle F_z \rangle_{pv}$ (cf. Appendix A) we find for

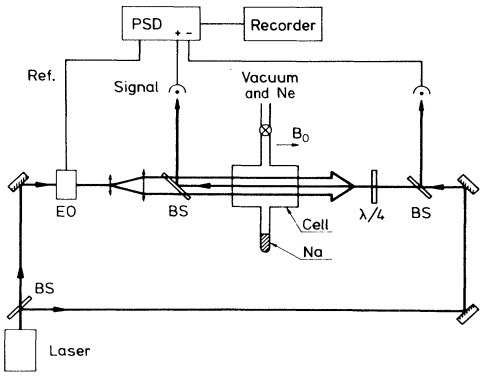

FIG. 2. Experimental setup for VSOP with orientation in sodium. Circular polarization of the expanded pumping beam is modulated by the electro-optic crystal (EO) from which a reference signal is sent to the lock-in amplifier (PSD). Probe beam is circularly polarized by a $\lambda/4$ plate. 50% beamsplitters are denoted by BS. Differential detection is used for an improved signal-to-noise ratio. Sodium cell is heated in an oven not shown in the figure. B_0 is a longitudinal magnetic field.

the effective saturation parameter $(\bar{\gamma}_p/\gamma_0)\langle F_z\rangle_{p\nu} \ll 1$. The detected signal is proportional to the orientation in the ground state and is sensitive to external transverse magnetic fields. The transverse fields in the cell were compensated by Helmholtz coils to within a few mG. An additional longitudinal field of 1 G was applied to force the resultant of the magnetic fields into the longitudinal direction.

A recording of the VSOP orientation spectrum of sodium in the absence of a foreign gas is shown in Fig. 3. The D_1 line ($3^2S_{1/2}-3^2P_{1/2}$, $I=\frac{3}{2}$) has $F_\mu=1,2$ and $F_\nu=1,2$. The four hyperfine structure resonances are displayed, as well as the crossover resonances appearing halfway in between any pair of direct resonances. The widths of the resonances are here determined by the natural widths of the transitions and the effective laser linewidth.

In Fig. 3 the spectrum is compared with the theoretical amplitudes of the orientation resonances calculated from (15) for the D_1 line of sodium at 150°C (cf. Appendix B, and a similar calculation in Ref. 24 for the case of polarization spectroscopy of sodium). Although the hyperfine structure leads to 16 terms in the sum over μ,ν in (15), these reduce to nine discrete resonances because of spectral coincidence. Note that one crossover signal vanishes as two resonant processes contribute with opposite signs and cancel. Good agreement with the experimental spectrum is found.

Since the relative magnitudes of the hyperfine resonances can be calculated accurately without any adjustable parameters, the spectrum measured in zero perturber gas pressure allows a check of possible systematic errors which might also distort collision line shapes. In fact, a closer analysis of several recorded hyperfine spectra revealed a slight relative attenuation of the resonances for the level $F_\nu=2$. The discrepancy could be attributed to absorption, which is strongest for $F_\nu=2$. This effect is discussed further in Sec. V.

B. Collision line shapes

When the cell is filled with a few millitorr of neon gas, collision effects appear in the VSOP spectra. The effective number of collisions per pumped atom depends on the pressure, and also on the diameter of the laser beams through the parameter γ_0. Orientation spectra of sodium were recorded at low neon

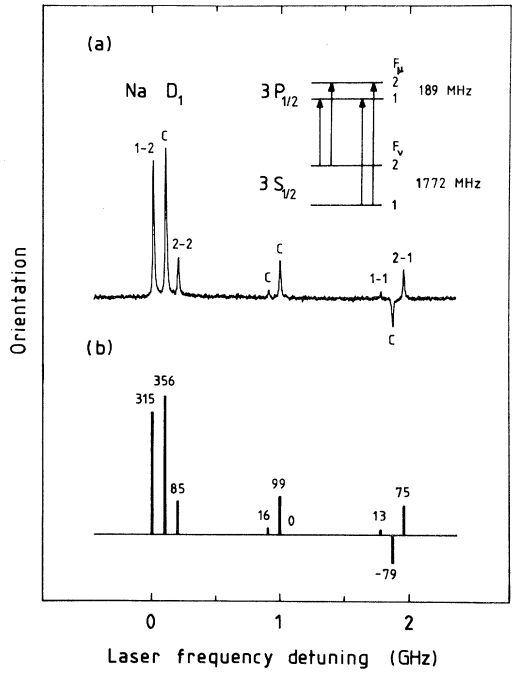

FIG. 3. The VSOP spectrum of the D_1 line of sodium obtained with orientation. (a) Experimental recording. Various hyperfine resonances are labeled by $F_\mu-F_\nu$ and the crossover signals by c. Inset shows the level structure with the hyperfine splittings and transitions of the D_1 line. (b) Theoretical spectrum. Relative peak heights calculated for 150°C are given.

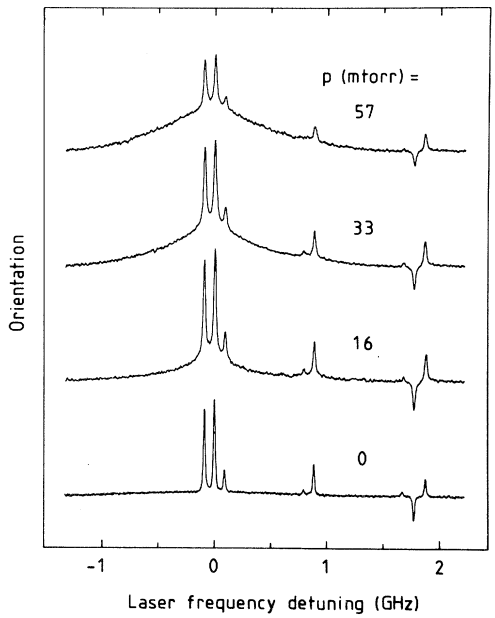

FIG. 4. Experimental VSOP line shapes of the D_1 hyperfine spectrum of sodium in various pressures of neon perturber gas. Vertical scales of the curves are not exactly equal but the figure serves for a qualitative comparison. Background produced by velocity-changing collisions is seen to be relatively narrow for 16 mtorr but is progressively broadened with increasing pressure. Resonances can be identified by comparing with Fig. 3.

pressures in the range of 0 to 57 mtorr, where only a few collisions contribute and the line profiles are still fairly sensitive to the shape of the kernel. Figure 4 shows recorded line shapes at various pressures of neon. A broad background distribution produced by velocity-changing collisions is seen to develop with increasing pressure.

The high-frequency side of the spectrum is seen to exhibit a very small collision background. This is because the crossover resonance with the common level $F_v=1$ gives a contribution of opposite sign which almost cancels that of the adjacent hyperfine resonances. The narrow peaks of these curves contain a slight residual Doppler broadening owing to a small crossing angle between the beams that was used in these measurements. The curves in Fig. 4 do not have precisely equal vertical scales but serve for a qualitative comparison.

In a pressure of 16 mtorr the pumped atoms undergo only one collision, on the average, before leaving the beam. This is seen by comparing the areas of the peaks and the background. This curve thus gives a crude image of the kernel involved. A relatively narrow central part of the distribution is seen under the peaks, revealing a substantial contribution from rather small velocity changes. With increasing pressure the background is rapidly broadened and increases in magnitude. The shape approaches the thermal equilibrium distribution at still higher pressure.

A quantitative analysis of the line shapes of Fig. 4 will be undertaken in Sec. V.

C. Modulated VSOP, the collision cross section

By applying rapidly modulated pumping (cf. Sec. II D) the rate γ_c for sodium-neon collisions was measured directly. The electro-optic modulator was driven at frequencies up to $\omega/2\pi=200$ kHz and the orientation signals were recorded in phase and in quadrature with the modulation of the polarization. The signals followed the behavior described by (26). The ratios $S_{\pi/2}/S_0$ of the in-quadrature and in-phase components of the Lorentzian peaks were measured. Figure 5 shows examples of $S_{\pi/2}/S_0$ plotted as a function of the modulation frequency for various pressures of neon. The straight lines are least-squares fits of the relation (27) to the experimental points. The deviations from linearity reflect mainly two types of experimental error: the uncertainty in measuring the strongly attenuated signals at high ω, and the instrumental inaccuracy in the measurement of the pressure.

The total relaxation rate γ is extracted from the slopes of the lines in Fig. 5 according to (27). Figure 6 shows a plot of the values obtained for γ as a function of pressure. The 10% inaccuracy in the pressure measurement is indicated by horizontal error bars. The vertical error bars represent the uncertainties of the fits in Fig. 5. The expected linear variation with pressure is found. A least-squares fit gives the values

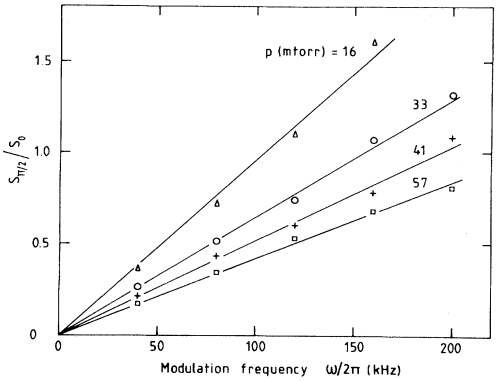

FIG. 5. Ratio of the in-quadrature and the in-phase components of the resonance peaks of the VSOP spectrum vs modulation frequency at various pressures of neon. Straight lines are least-squares fits to the experimental points.

$$\gamma_0=(3.21\pm0.25)\times10^5\ ,$$

where the units are s^{-1}, and

$$\gamma_c=(2.10\pm0.19)\times10^4 p\ ,$$

also in s^{-1}, with p in mtorr.

The total cross section σ for velocity-changing collisions is deduced from the relation $\gamma_c=N\sigma v_r$, where N is the number density of perturbers and v_r

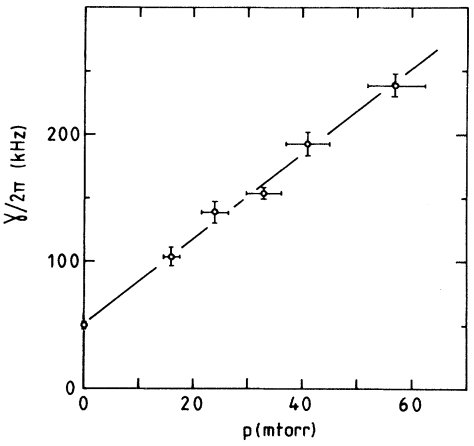

FIG. 6. Relaxation rate γ of the sodium atoms vs neon pressure. Vertical error bars represent statistical uncertainty, the horizontal bars give the inaccuracy of the pressure gauge. Straight line is the least-squares fit to the experimental points.

is the mean relative velocity between thermally distributed neon atoms and sodium atoms having zero axial velocity.[15] We obtain for sodium-neon collisions

$$v_r = 0.916(8k_BT/\pi\mu_r)^{1/2}, \quad (40)$$

where μ_r is the reduced mass and k_B is the Boltzmann constant. This yields the cross section

$$\sigma = (1.13 \pm 0.10) \times 10^{-14}$$

in units of cm^2. The measured value can be compared with the hard-sphere cross section based on atomic radii[25] for sodium and neon, which is $\sigma = 0.33 \times 10^{-14}$ cm^2. A value close to the latter has, in fact, been found to agree with experimental results on excited sodium atoms when the hard-sphere description was applied.[9] Our measurement of σ suggests that the hard-sphere model is not a satisfactory description of velocity-changing collisions in the ground state of sodium. It may be noted that our value of γ_c agrees with the collision-broadening rate for the D_1 line of sodium in neon perturber gas.[26]

V. COMPARISON WITH THEORY

Further information about the characteristics of the collisions was extracted from least-squares fits of phenomenological models to the VSOP line shapes. We have analyzed our data using the Keilson-Storer kernel as well as the two-term kernel (31).

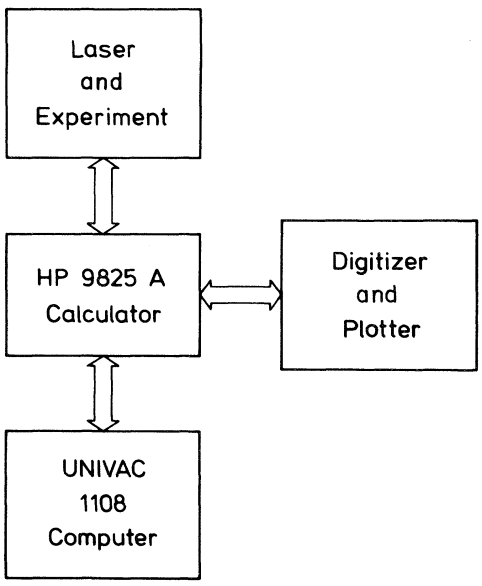

FIG. 7. Scheme of the computer system used for the analysis of the experimental VSOP line shapes.

For data processing the experiment was connected to a computer system as sketched in Fig. 7. The recorded spectra were sampled at 2000 points equally spaced on the frequency axis by the HP 9825A desktop computer, which also controlled the laser frequency tuning. The numerical analysis of the data was implemented on a UNIVAC 1108 computer.

To achieve a reasonable accuracy in the analysis it was necessary to take into account the following phenomena that cause systematic errors in the line shapes.

(a) The frequency-dependent absorption of the beams alters the relative magnitudes of the peaks and deforms the collision profile. This effect is taken into account by multiplying the theoretical signal by a frequency-dependent correction factor, which is calculated in Appendix C. For each recording the appropriate correction was determined by measuring the maximum absorption.

(b) A closer investigation reveals a broad residual background in the signal at zero pressure (see Fig. 4). This feature stems from the backward reflection of the pumping beam from the back window of the cell. The reflection gives rise to a weak pumping beam nearly copropagating with the probe beam. This effect requires an additional correction which is also given in Appendix C. The retroreflected pumping beam was measured to give a contribution of only 4% to the signal. However, because the backward reflected wave always gives broader background shapes than the main beam it was found to affect the analysis of the data.

(c) Nonlinearities in the frequency scan are produced by hysteresis effects in the galvanometer used for tuning and by thermal drift of the laser cavity length. The frequency scale was rectified by using a simultaneous record of the galvanometer position and by utilizing the hyperfine resonances as calibration marks. The remaining nonlinearity was estimated to be less than 1% of the full scan.

We note that fits were also attempted without these corrections, resulting in significantly larger errors than with the corrections included.

Because the disorienting effects of neon collisions on the sodium ground state are negligible in the present experiment[27] and the orientation survives until the atoms hit the cell wall, we could set $\xi = 1$.

For the Keilson-Storer model we used α, Γ_{eg}, and the ratio γ_c/γ_0 as adjustable parameters. In using the two-term kernel (31) the free parameters were α, Γ_{eg}, γ_c/γ_0, δ, and ϵ.

An inspection of the fits indicated that the Keilson-Storer model does not provide a satisfactory description of the experimental results. Firstly, the shapes of the theoretical collision backgrounds devi-

ate in details from the measured profiles, although the normalized least-squares errors were only about 3—10%. The deviation is demonstrated in Fig. 8(a), where the difference between the best fit of a Keilson-Storer shape and a curve measured at 33 mtorr is shown in a magnified scale. The Keilson-Storer shape has a shoulder too broad to fit the central part of the background. The sharp wiggles in the center of the curve result from a slight mismatch of the Lorentzian peaks due to an imperfect linearity of the scan. Secondly, the kernel width obtained from the fits appears to vary systematically with pressure instead of being constant: The value of α decreased from 0.75 to 0.63 with the pressure increasing from 16 to 57 mtorr.

For γ_c/γ_0, a linear increase with pressure was found as expected. Also, the values of Γ_{eg} tended to increase slightly with pressure.

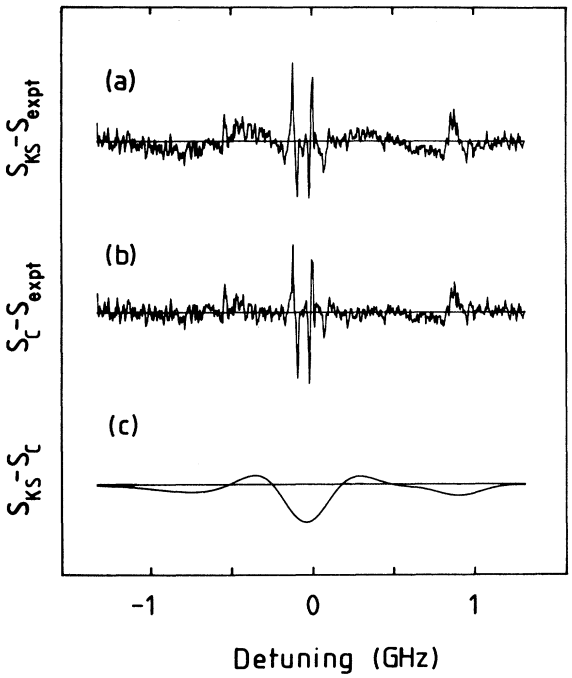

FIG. 8. This figure compares the experimental VSOP profile of sodium in 33 mtorr of neon with the fitted line shapes derived from the Keilson-Storer kernel and the composite kernel. (a) Difference between the Keilson-Storer profile S_{KS} and the experimental curve S_{expt}. (b) Difference between the profile of the composite model S_C and the experimental curve. (c) Difference between the collision backgrounds of the Keilson-Storer model S_{KS} and the composite model S_C (the resonances have been suppressed for clarity). Curve in (c) is seen to duplicate the systematic deviation of the background in (a). Note that the vertical scale is about ten times larger than that of Fig. 9.

It may be noted that the values of α yielding the best fits correspond to an rms velocity change per collision clearly smaller than that associated with a hard-sphere kernel for sodium-neon collisions.[8,9,17] To get the same persistence of velocity in the hard-sphere model and the Keilson-Storer model requires $\alpha=0.38$, but with this value the Keilson-Storer model overemphasizes the broadening and fails to reproduce the narrow central part of the profile at low pressures in our experiment. This discrepancy again suggests the presence of small velocity changes produced at larger values of the impact parameter.

The two-term collision model (39) was found to yield fits with smaller least-squares errors and better qualitative agreement with experiments than the Keilson-Storer model throughout the pressure range. In Fig. 8(b), the difference between the theoretical line shape of the two-term kernel and the experimental curve at 33 mtorr is shown. The two-term model clearly reproduces the details of the signal better than the Keilson-Storer model. This fact is further emphasized in Fig. 8(c), where the resonance peaks have been subtracted from both theoretical curves and the difference between the background shapes of the two theories has been drawn. The essential features of Fig. 8(a) are seen to be well reproduced. Figure 9 finally shows a fit of the two-term line shape to the experimental recording. The close agreement over the entire profile makes the two curves almost indistinguishable.

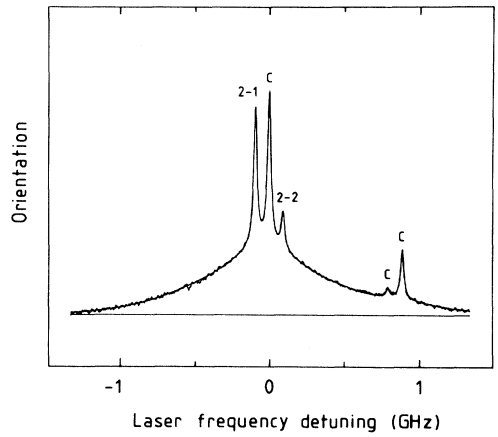

FIG. 9. Comparison of the collision profile derived from the composite (two-term) kernel with the experimental VSOP line shape of the sodium D_1 line. Measured curve (noisy line) is recorded at 33 mtorr of neon perturber gas. Maximum absorption of the beams was 25%. Theoretical curve (solid line) is a least-squares fit giving the parameter values (see the text) $\alpha=0.44$, $\delta/u=0.41$, $\epsilon=0.46$, $\Gamma_{eg}/ku=0.0162$, and $\gamma_c/\gamma_0=3.09$. Hyperfine components are labeled by $F_\mu-F_\nu$ and the crossover resonances by c.

With five free parameters, the fitting procedure became rather insensitive to variations in α and δ close to the optimum. This resulted in large fluctuations in the values of α, but without any evident systematic dependence on pressure. The values of δ appeared to increase with pressure but only within the error limits, whereas ϵ stayed fairly constant. Taking the total averages of α, δ, and ϵ over various pressures we found the following values for the parameters determining the two-term kernel shape:

$$\bar{\alpha}=0.37\pm0.15 ,$$

$$\bar{\delta}/u=0.39\pm0.07 ,$$

$$\bar{\epsilon}=0.51\pm0.12 ,$$

where the errors are standard deviations over 13 samples. These results were tested by fitting curves with the three kernel parameters fixed to their mean values. Throughout the pressure range these fits, obtained with the two free parameters Γ_{eg} and γ_c/γ_0, were still better than those obtained from the pure Keilson-Storer model, even when its kernel parameter α also was allowed to vary (three free parameters). In this sense the two-term kernel eliminates the unphysical dependence of the kernel parameters on pressure.

The values of Γ_{eg}/ku were found to increase from 0.0142 at 16 mtorr to 0.0168 at 57 mtorr. The ratio γ_c/γ_0 varied linearly from 1.33 to 5.87 over the pressure range. The slight increase in Γ_{eg} may indicate the presence of additional, very weak velocity-changing effects in the spectra. However, our experimental resolution was not sufficient to allow a closer investigation of a possible broadening of the peaks. At least part of the variation may follow from the coupling of parameters that cannot be avoided in a multidimensional fitting procedure.

The values of γ_c/γ_0 give the approximate number of collisions per atom. These values can be compared with the measured results of Sec. IV C, which yield $\gamma_c/\gamma_0=1.05$ at 16 mtorr with a linear increase to $\gamma_c/\gamma_0=3.73$ at 57 mtorr. The larger values obtained from the fits may be due to the fact that γ_0 depends on the pressure for the colliding atoms contributing to the background signal.[14] Also, with the relatively large value of δ obtained in the fit, the approximation included in (35) underestimates the broadening effects of several successive collisions. This may lead to an overestimation of the collision rate in the fit. Finally, the neglect of the velocity dependence of γ_c may contribute to the error as well.

It is interesting to note that the result for α is close to the value $\alpha=0.38$ obtained from the hard-sphere model.[8,9,17] It seems that the broader Keilson-Storer part of the kernel (31) may therefore be attributed mainly to the effects of close encounter collisions leading to large-angle scattering. As judged by our fits, the importance of the narrow part in the kernel apparently indicates a substantial contribution from collision interactions ranging beyond the hard-sphere radius.

VI. CONCLUDING REMARKS

In a VSOP experiment one detects well-defined atomic observables. In the linear optical-pumping regime, effects of saturation are absent, and the contributions to the line shape from the various hyperfine components are easy to account for theoretically. These features make the method convenient for a precise analysis of collision effects in the spectra. In this work we have presented the first application of VSOP for a detailed quantitative investigation of the effects of velocity-changing collisions on the line shapes. The measured observable was orientation but, because of the negligible depolarization in sodium-neon collisions, we expect our results on velocity-changing effects to be approximately valid for the entire density matrix of the sodium ground state.

In our analysis we have taken into account the finite absorption of the beams and the backward reflection of the pumping beam. These phenomena were found to have a noticeable effect on the shape of the spectrum.

By comparison of experimental line shapes with theoretical models, the Keilson-Storer kernel has been found unsatisfactory for a description of collisions between sodium atoms and neon perturbers. We have applied a collision model based on a two-term kernel to describe our experimental data. This model has been found to give an improved description of the observed effects of velocity-changing collisions in the VSOP spectra over the entire profile.

The following features emerge from our results:

(i) a Keilson-Storer kernel chosen to approximate hard-sphere collision effects ($\alpha=0.38$) does not fit well to the experimental line shapes;

(ii) the two-term model with a narrow part of the kernel chosen to describe a pronounced persistence of velocity was found to improve the fits significantly; and

(iii) the collision cross section obtained from the modulation experiment was considerably larger than the corresponding hard-sphere value.

These results suggest that the part of the interatomic potential ranging beyond the hard-core radius gives

an essential contribution to velocity-changing collisions.

Phenomenological studies of collision line shapes are useful for parametrizing the collision kernel or, strictly speaking, at least the collision data observed. A further development along these lines calls for a new ansatz for the collision kernel, possibly with an increased number of free parameters. However, even if it turned out that we could get a good description of the experimental results over the studied pressure range with a number of parameters fixed, adding new parameters may not seem an appealing approach. It would probably be more enlightening to bridge the gap between the collision kernel and the interatomic potential (cf. Refs. 9, 17, and 28).

ACKNOWLEDGMENTS

The authors are indebted to Professor E. Byckling for his support and encouragement. Valuable discussions with F. Laloë and M. Pinard are gratefully acknowledged by one of us (C.G.A). This work has been financially supported by the Academy of Finland.

APPENDIX A: THE PUMPING RATE COEFFICIENT

When $\gamma_p^{\mu\nu} \ll \gamma_0$ we can rewrite (3a) to the first order in the pumping rate by inserting $\rho_\nu^0(v)$ in the commutator and anticommutator of (3a) and on the rhs of (3b). By solving the steady state of (3b) and inserting into (3a) we have

$$\frac{d}{dt}\rho_\nu(v,t) = \sum_{\mu\nu'} \gamma_p^{\mu\nu'}(v) M_\nu^{\mu\nu'} \rho_{\nu'}^0(v) - \gamma_0[\rho_\nu(v,t) - \rho_\nu^0(v)] , \quad \text{(A1)}$$

where we have written the pumping operator using Kronecker's δ symbol:

$$M_\nu^{\mu\nu'} = A_\nu^{\mu\nu'} - B_{\mu\nu}\delta_{\nu\nu'} \quad \text{(A2)}$$

with

$$A_\nu^{\mu\nu'} = (\Gamma_{\mu\nu}/\Gamma_\mu) \sum_{i=xyz} P_\nu D_i P_\mu (\vec{e}_\lambda \cdot \vec{D}) \times P_{\nu'} (\vec{e}_\lambda^{\,*} \cdot \vec{D}) P_\mu D_i P_\nu . \quad \text{(A3)}$$

The operator $A_\nu^{\mu\nu'}$ describes the transition from the level $F_{\nu'}$ to F_μ by absorption followed by decay to F_ν through spontaneous emission. The branching ratio of the spontaneous decay is $\Gamma_{\mu\nu}/\Gamma_\mu$. $B_{\mu\nu}$ is defined by (6) and gives the effect of absorption on the level F_ν.

Equation (9) describing the evolution of $\langle F_z \rangle_\nu(v)$ is obtained from (7), (8), and (A1). The source term (12) contains the pumping coefficients defined by

$$\langle F_z \rangle_{p\nu}^{\mu\nu'} = \mathrm{Tr}_\nu\{F_z M_\nu^{\mu\nu'}\}/(2I+1)(2J_g+1) . \quad \text{(A4)}$$

Because the dipole operator $\vec{D}$ acts only on the state of the electron we obtain the matrix elements of $\vec{D}$ as[29]

$$\langle F_\mu m_\mu \mid D_q \mid F_\nu m_\nu \rangle = (-1)^{1+I+J_g+F_\mu}[(2J_e+1)(2F_\nu+1)]^{1/2} \times \begin{Bmatrix} 1 & F_\nu & F_\mu \\ I & J_e & J_g \end{Bmatrix} \langle F_\nu 1 m_\nu q \mid F_\mu m_\mu \rangle , \quad \text{(A5)}$$

where $m_{\mu,\nu}$ labels the magnetic substates of the hyperfine states $F_{\mu,\nu}$.

APPENDIX B: SIGNAL STRENGTHS FOR HYPERFINE-STRUCTURE COMPONENTS

To calculate the transmitted intensity of the σ_+ polarized detection beam we apply the results given in the Appendix of Ref. 2 to an atom with hyperfine structure. The absorption of the probe beam depends only on the density matrix of the ground state, and each hyperfine component $F_\nu \rightarrow F_\mu$ will contribute to the absorption by

$$S_{\mu\nu} \propto \frac{|\mathscr{E}_d|^2 |\mathscr{D}_{eg}|^2}{2J_e+1} \int_{-\infty}^{\infty} dv\, \mathrm{Tr}_\nu\{\rho_\nu(v) B_{\mu\nu}^{(+)}\} \times L(\Omega - \Omega_{\mu\nu} + kv) , \quad \text{(B1)}$$

where $B_{\mu\nu}^{(+)}$ is the absorption operator (6) with σ_+ polarization, $\vec{e}_\lambda = \vec{e}_+$. In using polarization modulation between the σ_+ and σ_- states (equivalently in the pumping or detection beam) and phase-sensitive detection, the signal is proportional to

$$\mathrm{Tr}_\nu\{\rho_\nu(v)(B_{\mu\nu}^{(+)} - B_{\mu\nu}^{(-)})\} = \sqrt{2}\langle T_0^{(1)}(F_\mu)\rangle_\nu(v) , \quad \text{(B2)}$$

where we have used the development of $B_{\mu\nu}$ into irreducible tensor operators[30] and $T_0^{(1)}$ is the standard tensor component proportional to the orientation. The matrix elements of the F_μ-dependent operator $T_0^{(1)}(F_\mu)$ in the hyperfine state subspace are evaluated using the result of Ref. 29. We obtain the signal proportional to the orientation in the form

$$S_{\mu\nu}(\Omega) \propto \frac{|\mathscr{E}_d|^2 |\mathscr{D}_{eg}|^2}{2J_e+1} R_{\mu\nu}^{(1)} \times \int_{-\infty}^{\infty} dv \langle F_z \rangle_\nu(v) L(\Omega - \Omega_{\mu\nu} + kv) , \quad \text{(B3)}$$

where

$$R^{(1)}_{\mu\nu}=(-1)^{1+F_\mu+F_\nu}(2F_\mu+1)\left[\frac{2F_\nu+1}{F_\nu(F_\nu+1)}\right]^{1/2} \times \begin{Bmatrix} F_\nu & F_\nu & 1 \\ 1 & 1 & F_\mu \end{Bmatrix} \begin{Bmatrix} 1 & F_\nu & F_\mu \\ I & J_e & J_g \end{Bmatrix}^2 . \tag{B4}$$

Summing (B3) over μ and ν gives the total orientation signal (14).

The relative strengths of the various hyperfine and crossover resonances are given by the coefficients $Q^{\mu'\nu'}_{\mu\nu}$ in (16), and are calculated from (B4) and (A4) by using (A2), (A3), (6), and (A5).

For the D_1 line of sodium the hyperfine states are $F_\mu,F_\nu=1,2$. For the convenience of notation we relabel the pairs (μ,ν) by the running index i in the order of ascending frequencies of the hyperfine transitions as $(1,2)\rightarrow 1$, $(2,2)\rightarrow 2$, $(1,1)\rightarrow 3$, and $(2,1)\rightarrow 4$. We then obtain

$$Q^{i'}_i = C \begin{bmatrix} 315 & 255 & 45 & 225 \\ 105 & 85 & 15 & 75 \\ -5 & 15 & 13 & -15 \\ 25 & -75 & -65 & 75 \end{bmatrix} , \tag{B5}$$

where the row and column indices run over i and i', respectively, and C is a numerical factor.

APPENDIX C: CORRECTIONS

1. Correction for absorption

The attenuation of the intensity I of the detection beam propagating along the z axis through the vapor cell is described by

$$\frac{d}{dz}I(z)=-a(z)I(z) , \tag{C1}$$

where the absorption depends on the pumping beam intensity I_p to first order:

$$a(z)=a_0+q_\lambda I_p(z) . \tag{C2}$$

The unperturbed absorption coefficient is a_0, and q_λ describes the optical-pumping effect. The counterpropagating pumping beam $I_p(z)$ is given by

$$I_p(z)=I_p e^{-a_0(L-z)} \tag{C3}$$

in a cell of length L. The detection beam intensity is solved from (C1), (C2), and (C3):

$$I(z)=I_0\exp[-a_0 z-q_\lambda I_p e^{-a_0 L}(e^{a_0 z}-1)/a_0] . \tag{C4}$$

In a measurement of the circular dichroism created with a $\sigma_\pm$ modulated pumping polarization the signal is given by

$$S=I(L,q_+)-I(L,q_-) . \tag{C5}$$

With a circularly polarized probe beam the pumped dichroism is described by $q_+=-q_-=q$. Assuming $|qI_p/a_0|\ll 1$ we obtain

$$S=2I_0 I_p q e^{-a_0 L}(1-e^{-a_0 L})/a_0 . \tag{C6}$$

This determines the correction factor $g(\Omega)$ for the VSOP line shape:

$$g(\Omega)=e^{-a_0(\Omega)L}(1-e^{-a_0(\Omega)L})/a_0(\Omega)L , \tag{C7}$$

where $a_0(\Omega)$ is the Doppler profile of the entire hyperfine multiplet for linear absorption in an optically thin sample.

For the D_1 line of sodium, the function $a_0(\Omega)$ may be closely approximated by

$$a_0(\Omega)=A\left\{\exp\left[-\left[\frac{\Omega-\frac{1}{2}(\Omega_{12}+\Omega_{22})}{ku}\right]^2\right]+0.6\exp\left[-\left[\frac{\Omega-\frac{1}{2}(\Omega_{21}+\Omega_{11})}{ku}\right]^2\right]\right\} , \tag{C8}$$

where A is chosen to give the measured maximum absorption.

2. Correction for retroreflected pumping beam

The reflection of the pumping beam from the back window of the cell gives rise to an additional beam. This produces optical pumping with the rate $r\bar{\gamma}_p$, where r is an effective reflection coefficient including, e.g., geometric factors from misaligned beams. The reflected beam approximately copropagates with the probe beam and produces a weak orientation $\langle F_z\rangle^r_v(v)$, calculated from (20) by changing k into $-k$. The corresponding correction to the signal is obtained from (14) with $\langle F_z\rangle_v$ replaced by $\langle F_z\rangle^r_v$:

$$S_r(\Omega)\propto r\frac{\bar{\gamma}_p}{\gamma}\sum_{\mu\nu}\sum_{\mu'\nu'}Q_{\mu\nu}^{\mu'\nu'}\exp\left[-\left[\frac{\Omega-\Omega_{\mu'\nu'}}{ku}\right]^2\right]\left[1+2\pi\frac{\Gamma_{eg}}{k\gamma}\sum_{n=1}^{\infty}K^{(n)}(-v_{\mu'\nu'},-v_{\mu\nu})\right]. \tag{C9}$$

The total signal is then given by $S_{\rm tot}(\Omega)=S(\Omega)+S_r(\Omega)$, where $S(\Omega)$ is obtained from (23). The correction is seen to add a thermal and a nonthermal contribution.

For illustration, we give $S_{\rm tot}$ for a two-level transition with the Keilson-Storer kernel applied:

$$S_{\rm tot}(\Omega)\propto\exp\left[-\left[\frac{\Omega-\Omega_0}{ku}\right]^2\right]\left\{L(\Omega-\Omega_0)+r+2\sqrt{\pi}\frac{\Gamma_{eg}}{ku}\sum_{n=1}^{\infty}\eta^n(1-\alpha^{2n})^{-1/2}\times\left\{\exp\left[-\left[\frac{\Omega-\Omega_0}{ku}\right]^2\left[\frac{1+\alpha^n}{1-\alpha^n}\right]\right]+r\exp\left[-\left[\frac{\Omega-\Omega_0}{ku}\right]^2\left[\frac{1-\alpha^n}{1+\alpha^n}\right]\right]\right\}\right\}. \tag{C10}$$

The reflected beam is seen to broaden the line shape. The constant r can be determined from a measurement in zero perturber pressure ($\eta=0$).

[1]M. Pinard, C. G. Aminoff, and F. Laloë, Phys. Rev. A 19, 2366 (1979); M. Pinard, Thèse, Université Paris VI, 1980 (unpublished).

[2]C. G. Aminoff and M. Pinard, J. Phys. (Paris) 43, 263 (1982).

[3]P. R. Berman, Adv. At. Mol. Phys. 13, 57 (1977).

[4]V. P. Chebotaev and L. S. Vasilenko, Prog. Quantum Electron. (in press).

[5]J. P. Barrat and C. Cohen-Tannoudji, J. Phys. Radium 22, 329 (1961); 22, 443 (1961).

[6]C. Brechignac, R. Vetter, and P. R. Berman, J. Phys. B 10, 3443 (1977); Phys. Rev. A 17, 1609 (1978); J. Phys. (Paris) Lett. 39, L-231 (1978).

[7]Ph. Cahuzac, O. Robaux, and R. Vetter, J. Phys. B 9, 3165 (1976).

[8]J-L. LeGouët, J. Phys. B 11, 3001 (1978).

[9]P. F. Liao, J. E. Bjorkholm, and P. R. Berman, Phys. Rev. A 21, 1927 (1980).

[10]W. Happer, Rev. Mod. Phys. 44, 169 (1972).

[11]T. W. Hänsch, I. S. Shahin, and A. L. Schawlow, Phys. Rev. Lett. 27, 707 (1971).

[12]P. G. Pappas, R. A. Forber, W. W. Quivers, Jr., R. R. Dasari, M. S. Feld, and D. E. Murnick, Phys. Rev. Lett. 47, 236 (1981).

[13]A possible broadening of the homogeneous linewidth by phase-changing collisions is assumed small and is included in Γ_{eg}.

[14]The relaxation model implied in γ_0 is somewhat simplistic. Initially γ_0 was assumed to reflect the time of free flight through the beam. We expect that this model for γ_0 applies to the Lorentzian peaks resulting from atoms that have not yet collided. On the contrary, the atoms redistributed by collisions should be associated with a γ_0 decreasing with pressure, corresponding to the diffusion of atoms through the cell.

[15]J. Julien, Thèse, Université Paris VI, 1981 (unpublished).

[16]J. Keilson and J. E. Storer, Q. Appl. Math. 10, 243 (1952).

[17]M. Borenstein and W. E. Lamb, Jr., Phys. Rev. A 5, 1311 (1972).

[18]Ph. Cahuzac, E. Marié, O. Robaux, R. Vetter, and P. R. Berman, J. Phys. B 11, 645 (1978).

[19]M. Gorlicki, A. Peuriot, and M. Dumont, J. Phys. (Paris) Lett. 41, L-275 (1980).

[20]J.-L. LeGouët and P. R. Berman, Phys. Rev. A 17, 52 (1978).

[21]In order to keep our result (23) for the signal valid we will also assume $\Gamma_{eg}\ll k\delta$.

[22]M. Pinard, C. G. Aminoff, and F. Laloë, Appl. Phys. 15, 371 (1978); see also C. G. Aminoff and M. Kaivola, Opt. Commun. 37, 133 (1981); Appl. Phys. B 26, 133 (1981).

[23]Although the probe intensity is not much weaker than the pumping intensity, the pumping effect of the probe beam can be neglected, as the low intensities assure a linear optical-pumping regime and then only the effect of the modulated pumping beam is observed with lock-in detection.

[24]S. Nakayama, J. Phys. Soc. Jpn. 50, 609 (1981).

[25]C. W. Allen, *Astrophysical Quantities,* 3rd ed. (University of London, London, 1973), p. 45.

[26]D. G. McCartan and J. M. Farr, J. Phys. B 9, 985 (1976).

[27]L. W. Anderson and A. T. Ramsay, Phys. Rev. 132, 712 (1963).

[28]S. Avrillier, C. J. Bordé, J. Picart, and N. Tranh Minh, J. Phys. (Paris) 43, 1213 (1982); S. Avrillier, Thèse, Université Paris-Nord, 1978 (unpublished).

[29]F. Laloë, M. Leduc, and P. Minguzzi, J. Phys. (Paris) 30, 277 (1969).

[30]C. Cohen-Tannoudji and F. Laloë, J. Phys. (Paris) 28, 505 (1967); 28, 722 (1967).